OXFORD

Cerebral Cortex, 2023, **33**, 421–433
https://doi.org/10.1093/cercor/bhac075
Advance access publication date 10 March 2022
Original Article

Distinct cerebral coherence in task-based fMRI hyperscanning: cooperation versus competition

Le-Si Wang[1], Jen-Tang Cheng[2], I-Jeng Hsu[2], Shyhnan Liou[1], Chun-Chia Kung[3,4,*,†], Der-Yow Chen[3,4,*,†], Ming-Hung Weng[2,*,†]

[1]Institute of Creative Industries Design, National Cheng Kung University (NCKU), No. 1, University Road, Tainan City 701, Taiwan,
[2]Department of Economics, NCKU, No. 1, University Road, Tainan City 701, Taiwan,
[3]Department of Psychology, NCKU, No. 1, University Road, Tainan City 701, Taiwan,
[4]Mind Research and Imaging (MRI) Center, No. 1, University Road, Tainan City 701, Taiwan
*Corresponding authors: Department of Psychology, National Cheng Kung University, No.1, University Road, Tainan City 701, Taiwan. Email: cckung@kunglab-nckupsy.org (C-CK); Department of Psychology, National Cheng Kung University, No.1, University Road, Tainan City 701, Taiwan. Email: chendy@ncku.edu.tw (D-YC); Department of Economics, National Cheng Kung University, No.1, University Road, Tainan 701, Taiwan. Email: mhweng@ncku.edu.tw (M-HW)

†These authors contributed equally to this work.

This study features an functional magnetic resonance imaging (fMRI) hyperscanning experiment from 2 sites, 305 km apart. The experiment contains 2 conditions: the dyad collaborated to win and then split the reward in the cooperation condition, whereas the winner took all the reward in the competition condition, thereby resulting in dynamic strategic interactions. To calculate the cerebral coherence in such jittered event-related fMRI tasks, we first iteratively estimated the feedback-related blood oxygenation level-dependent responses of each trial, using 8 finite impulse response functions (16 s) and then concatenated the beta volume series. With the right temporal–parietal junction (rTPJ) as the seed, the interpersonal connected brain areas were separately identified: the right superior temporal gyrus (rSTG) (cooperation) and the left precuneus (lPrecuneus) (competition), both peaking at the designated frequency bin (1/16 s = 0.0625 Hz), but not in permuted pairs. In addition, the extended coherence analyses on shorter and longer concatenated volumes verified that only in the optimal trial frequency did the rTPJ–rSTG and rTPJ–lPrecuneus couplings peak. In sum, our approach both showcases a flexible analysis method that widens the applicability of interpersonal coherence in the rapid event-related fMRI hyperscanning and reveals a context-based inter-brain coupling between interacting pairs during cooperation and during competition.

Key words: functional connectivity; functional magnetic resonance imaging (fMRI); hyperscanning; interpersonal coherence; strategic cheap talk game.

Introduction

In recent years, social neuroscience has been one of the fast growing fields among branches of functional neuroscience, partly due to the emerging consensus about its importance in the ever-changing world, from interpersonal to global contexts, prompting for the underlying mechanisms and ensuing remedies/interventions from the neuroscientific viewpoints. Not surprisingly, most of the queries of social neuroscience have to be "social," or interactions between 2 or among more people or agents in nature, to be categorized as "social neuroscientific." Various research paradigms, tools, and analytic methods have helped expand the breadth and depth of its inquiries. Two recent reviews summarized the growth, outstanding work, and the challenges ahead for social neuroscientists using hyperscanning (Redcay and Schilbach 2019; Misaki et al. 2021), a popular method characterized by having one or more neuroimaging devices synchronously or asynchronously, making optimized social inquiries. After listing the advent of the first hyperscanning paper (Montague et al. 2002) and ensuing publications, one of the shortcomings revealed in both Misaki et al. (2021) and Redcay and Schilbach (2019) is the relative scarce of real hyperscanning functional magnetic resonance imaging (fMRI) studies, and the limited analysis methods thereof. The reason may be obvious: the technical feasibility and the collaborations among highly skilled teams required for hyperscanning are not easy for any individual fMRI labs. To fill in the gaps, we (several fMRI practitioners in southern Taiwan) have developed an internet-based hyperscanning, similar to the earlier pioneering work (King-Casas et al. 2005) that featured the 2 (or more) computers connected to a central server, receiving from and sending to client computers the signals for achieving synchronous onset triggers. By over a hundred times of hyperscanning experiments, this fMRI study marks the beginning of fruition after years of our accumulated work.

As one of the important methods that characterize social neuroscientific studies using hyperscanning

Received: August 6, 2021. **Revised:** January 27, 2022. **Accepted:** January 29, 2022

(Czeszumski et al. 2020; Misaki et al. 2021), cerebral coherence is a spectral measure that estimates the linear time-invariant relationship between (intra- or) interpersonal time series, with maps of task- or condition-specific connectivity associated with seed (or electrode) regions of interest. Because of its insensitivity to slight temporal lags, which happen regularly in common social interactions, cerebral coherence has been one of the desirable choices to reveal inter-brain communications among seas of 2 (or more) electroencephalogram (EEG)/magnetoencephalography (MEG)/functional near-infrared spectroscopy (fNIRs)/fMRI signals (Mu et al. 2016; Nguyen et al. 2020; Yang et al. 2020; Chholak et al. 2021). However, due to both the technical challenges in conducting fMRI hyperscanning and the methodological constraints to meet coherence analyses (detailed next), to date there is only one (Stolk et al. 2014) publication of fMRI hyperscanning studies employing coherence analysis, with a decent number of hyper-fNIRs, -ERP, or even -MEG studies (Baillet 2017; Novembre et al. 2017; Ahn et al. 2018; Zhang et al. 2019) reporting coherence analyses. The reasons are probably due to the following: (i) cerebral coherence relies on time-to-frequency domain (e.g. Fourier) transformation, which requires the periodicity (or fixed intervals) of events/conditions to begin with. In contrast, most task-fMRI studies, especially event-related ones, were realized by irregular inter-trial intervals; (ii) coherence typically requires the long task condition/runs, whereas most fMRI studies intermix several conditions of interest, each with variable numbers of blocks or short-duration (approximately <20 s) trials presented in an unpredictable manner, adding another layer of complexity; (iii) most importantly, despite its early onset (Montague et al. 2002), hyperscanning remains technically formidable. Some labs may have resolved the difficulty of long-distance (internet) communications by close-by fMRIs in research institutes (Bilek et al. 2015) or hospitals, but the cost–benefit analysis still deters researchers from striding into these challenges.

To fill this lack of hyperscanning fMRI studies with coherence analyses, driven by the conflicts between requirements with different experimental designs (preferring short trials) and analysis methods (preferring long brain volumes), we tried to "have the cake and eat it too," by designing a jittered event-related hyperscanning fMRI study, adopting both the conventional GLMs, other derived analyses such as connectivity and multivariate mappings (Shen et al. 2021), and the cerebral coherence analyses in the present study. To do so, we adopted the method that Turner et al. (2012) introduced (the Turner method hereafter) in preparing our feedback-evoked volume time series. The Turner method is an iterative least squares-separate method aiming to unmix overlapping blood oxygenation level-dependent (BOLD) responses of adjacent events, due to the hemodynamic delay commonly seen in most jittered event-related fMRI designs. Its precedent, the paper by Mumford et al. (2012) (the Mumford method hereafter), demonstrates that in jittered event-related fMRI, its single-trial beta estimates yield the highest multivariate classification accuracy. The Turner method, in contrast, estimates multiple parameters (8 betas in our case, 1 beta per TR, which were later concatenated into a long volume time series, ready for the coherence analyses) per trial by estimating BOLD responses from a series of finite impulses, capturing more temporal dimensions than offered by the Mumford counterpart.

To test and validate the idea of using this transformed beta-concatenated time series for coherence analysis, a task-based fMRI experiment was implemented while subjects cooperated (and split the reward) or competed (and the winner took all) in a strategic cheap talk game (Crawford and Sobel 1982; see Section 2). The feedback period of the cooperation condition was especially of interest, since it was the time during which the dyads verified and strengthened their mutual understanding. Significant increases in interpersonal coherence between right temporal–parietal junction (rTPJ) and right superior temporal gyrus (rSTG) were identified, resembling past findings from the relevant literature (Stolk et al. 2014; Bilek et al. 2015; Jahng et al. 2017; Goelman et al. 2019). That is, there was significant interpersonal coherence between rTPJ and rSTG during the feedback period of the cooperating pairs, but not the randomly permuted ones. To our knowledge, this is the first study implementing coherence analysis on a task-based jittered event-related fMRI experiment. It therefore increases the generalizability of the coherence analysis and provides extra information alongside findings from other types (e.g. univariate and multivariate) of task-based analysis methods.

Materials and methods

Participants

Thirty-three pairs of participants between 20 and 30 years of age ($M = 23.4$, $SD = 2.9$) were recruited from National Taiwan University (NTU) and National Cheng Kung University (NCKU), situated in northern and southern Taiwan, respectively. All participants were native Taiwanese speakers, with normal or corrected-to-normal vision, and reported no history of psychiatric or neurological disorders. Participants gave written informed consent and adhered to the relevant guidelines and regulations approved by the NCKU Governance Framework for Human Research Ethics https://rec.chass.ncku.edu.tw/en, with the case number 106-254.

Experimental task

The strategic task in the present hyperscanning experiment mimicked the "cheap talk" game (Crawford and Sobel 1982), a special version of signaling games (Spence 1973) where the signal was made with costless communication. Participating dyads interacted sequentially either as the Sender or the Receiver to determine who would earn the reward. The talk (signal) was "cheap" not only because it was costless but also because it would be

uninformative except when the interests of the Sender and the Receiver were positively aligned.

Participants recruited to either site were assigned pseudorandomly as Player 1 or 2. They learned the rules of the game during separate briefings without being instructed on the appropriate way of playing and had completed a short practice session before the formal scanning. At the beginning of each trial, there were 2 boxes presented, only one containing the target reward. Participants knew in which condition and what role they were (as the Sender or the Receiver), from the information shown at the beginning of each trial. Their objective was to choose the correct box so to either split (in the cooperation or "$200" condition, Fig. 1A) or take all (in the competition or "$150" condition, Fig. 1B) the reward. When acting as the Sender, the participant alone was informed of the probabilities of money in both boxes (in pie charts) and was told to suggest which box the Receiver should open. After viewing the suggestion from the Sender, the Receiver subsequently selected which box to open. In all trials, the box chosen by the Receiver was the final decision for both. In the "200" condition, the dyad split the NT$200 reward if the chosen box was with the money. As their interests were perfectly aligned, the dyad was expected to fully cooperate in order to split the reward. On the other hand, in the "150" condition, the Receiver opened the chosen box, and the Sender got the unchosen one. The fact that only one would get the NT$150 reward caused a conflict between the dyad, who would then be engaged in the strategic competition. To balance the expected rewards in these 2 conditions, the cooperation condition was set to have a 75% success rate, meaning that even though the dyads cooperated nearly 100% of the trials, their winning probability was set to be 75%, or 3 out of every 4 trials. Therefore, the expected reward for each person was ($200 × 75%)/2 (splitting) = $75. Whereas in the competition condition, each was expected to win with equal chance (50%), so that the expected reward for each player was also the same ($150 × 50% = $75). Participants were aware that their bonus would depend on the rewards they had won from one randomly selected trial, in addition to a financial payment of NT$600 (~US$20), to compensate for their time in the experiment.

A 2-by-2 manipulation of "cooperation ($200) versus competition ($150)" and "Sender (S) versus Receiver (R)" was administered in an alternating fashion (Fig. 1C). The players changed their roles after every 2 trials while conditions alternate between cooperation and competition. Sequences of $200S-$150S-$200R-$150R for Player 1 and $200R-$150R-$200S-$150S for Player 2 repeated to make up the 28 trials of each run. The order of conditions was fixed across dyads, each of whom took approximately 70 min to finish all 4 runs. Each trial lasted 17 s: 3 s for the Sender's decision, 4 s of fixation, 3 s for the Receiver's decision, 4 s of fixation, and 3 s of feedback. The inter-trial interval was approximately 3–9 s.

fMRI data acquisition and preprocessing

The fMRI images of senders and receivers were acquired simultaneously in 2 MRI scanners, one in NCKU Tainan, another in NTU Taipei, 305 km apart. The MRI scanner at NCKU Mind Research and Imaging Center is a 3-Tesla General Electric Discovery MR750 (GE Medical Systems, Waukesha, WI), equipped with an 8-channel head coil. Whole-brain functional scans were acquired with a T2* EPI (time repetition [TR] = 2 s, time echo [TE] = 33 ms, flip angle = 90°, 40 axial slices, voxel size = 3.5 × 3.5 × 3 mm^3). High-resolution T1-weighted structural scans were acquired using a 3D fast spoiled grass (FSPGR) sequence (TR = 7.65 ms, TE = 2.93 ms, inversion time = 450 ms, final alignment [FA] = 12°, 166 sagittal slices, voxel size = 0.875 × 0.875 × 1 mm^3). Another fMRI scanner, which is located at NTU (Imaging Center for the Body, Mind, and Culture Research) is a 3-Tesla PRISMA (Siemens, Erlangen, Germany) scanner equipped with a 20-channel phase array coil. Whole-brain functional scans were acquired with a T2*-weighted EPI (TR = 2 s, TE = 24 ms, flip angle = 87°, 36 axial slices, voxel size = 3 × 3 × 3 mm^3). High-resolution T1-weighted structural scans were acquired using a magnetization-prepared rapid gradient-echo (TR = 2.0 s, TE = 2.3 ms, inversion time = 900 ms, FA = 8°, 192 sagittal slices with 0.938 × 0.938 × 0.94 mm^3 voxels without an interslice gap). The fMRI data were preprocessed and analyzed using BrainVoyagerQX v. 2.6 (Brain Innovation, Maastricht, The Netherlands) and NeuroElf v1.1 (https://neuroelf.net). After slice timing correction, functional images were corrected for head movements using the 6-parameter rigid transformations, aligning all functional volumes to the first volume of the first run. High-pass temporal filtering (with the default BVQX option of GLM-Fourier basis set at 2 cycles per degree, no spatial smoothing) was applied. The resulting functional data were co-registered to the anatomical scan via initial alignment and FA, and then both functional (*.fmr) and anatomical (*.vmr) files were transformed into Talairach space.

Before proceeding to cross-site coherence analysis, we examined whether imaging data acquired from the 2 different scanners (GE MR750 in NCKU and Siemens Prisma in NTU) had produced comparable quality, especially those specific ROIs we were interested in Supplementary Figure 1A exhibited similar distributions of estimated beta in rTPJ across the 2 sites. Moreover, Supplementary Fig. 1B demonstrated the 2 closely aligned distributions of coherence with rTPJ from each site as the seed ROI and rSTG in the counterpart as the target ROI. Their highly close means and SDs lend confidence to the relative comparability of (both the input and output of) the coherence analyses.

Data preparation and the coherence analysis

The procedures of converting an event-related jittered fMRI dataset into a format ready for coherence analysis are detailed in Fig. 2. First, only the feedback period of any given trial (here the cooperation, or $200, condition,

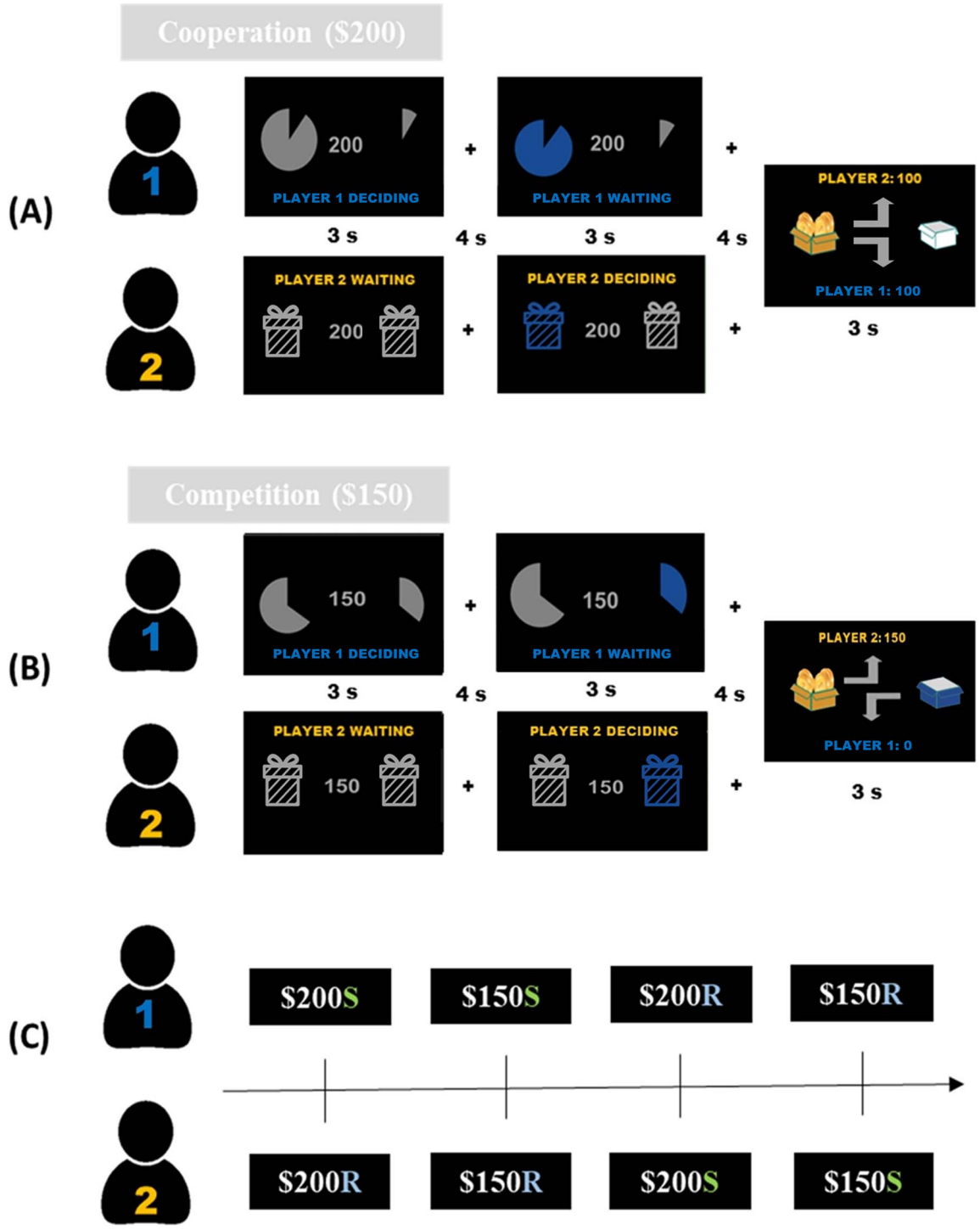

Fig. 1. The schematic of the present hyperscanning experiment and its possible scenarios. In both types of the strategic interaction, the Sender (Player 1), knowing the probability of the treasure box, first suggested a box for the Receiver (Player 2) to open. Observing the suggestion, the Receiver subsequently made the decision of which box to open. A) In the cooperation ($200) condition, the Sender suggested opening the box with a higher chance of winning the reward, the Receiver then followed the suggestion, and the 2 successfully split the NT$ 200 reward. B) In the competition condition ($150), the Sender suggested the box with a lower winning chance, but the Receiver did not follow the suggestion. In the end, the reward was in the box opened by the Receiver, who won the reward of NT$150 alone, and the Sender obtained nothing. C) The 2-by-2 manipulation, "cooperation vs. competition" and "Sender vs. Receiver," was arranged in an alternating fashion. These sequences repeated to make up the 28 trials of each run (4 runs in total).

was used for analysis (Fig. 2A). Next, as shown in Fig. 2B, the protocol response time of an fMRI run (totally 4 runs), along with the voxel time series, was created. Each run's protocol file (check the "PRT" folder under each pair in https://osf.io/f75cp/) contained 7 regressors as follows:

(1) con_200_1st = "condition NT$ 200 in the cooperation condition, 1st as the Sender";

(2) con_200_2nd = "condition NT$ 200 in the cooperation condition, 2nd as the Receiver";

(3) con_150_1st = "condition NT$ 150 in the competition condition, 1st as the Sender";

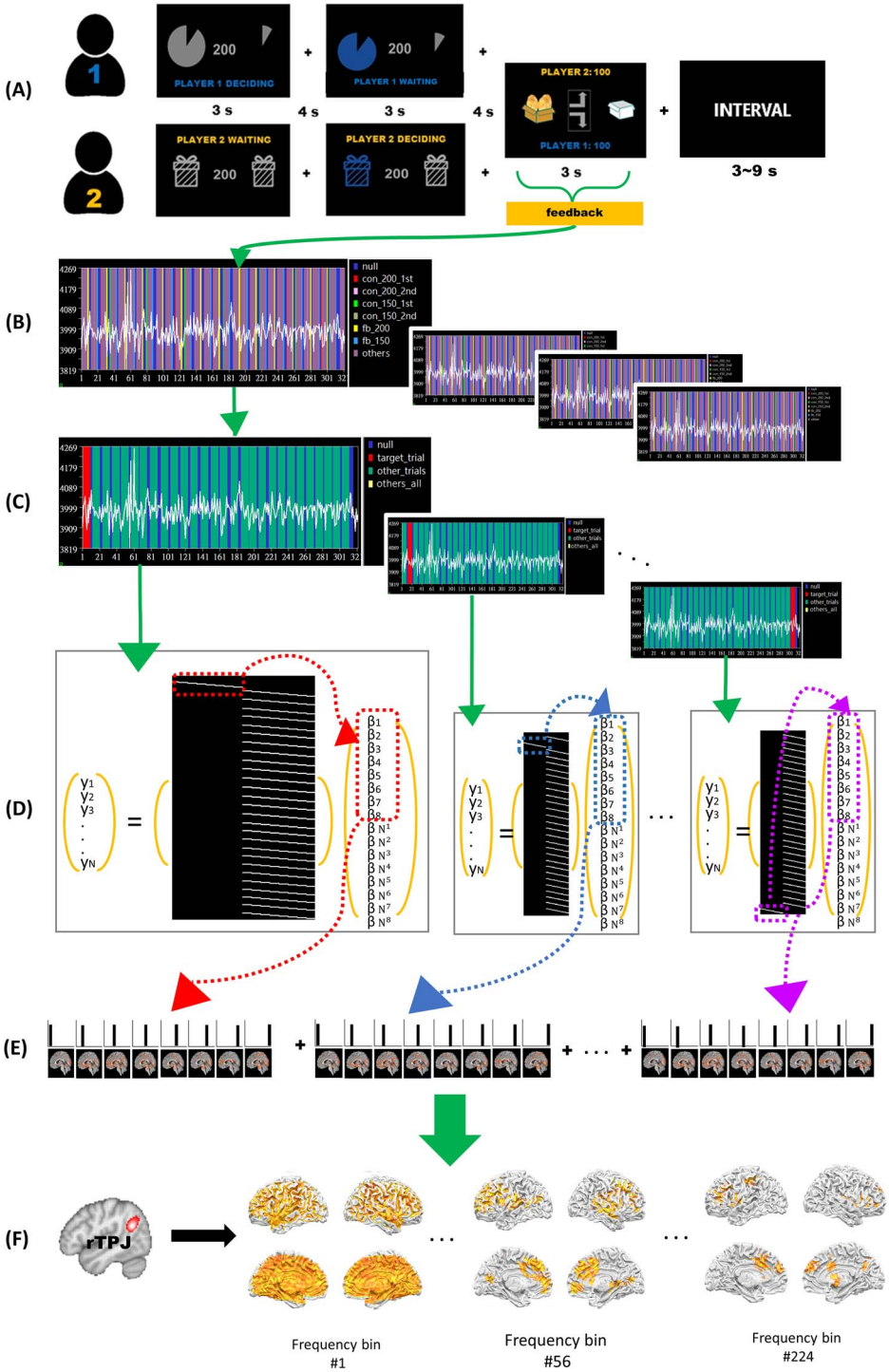

Fig. 2. The schematic procedure of converting an event-related jittered fMRI dataset into a format ready for coherence analysis. A) The interpersonal coherence in the present study focused on the brain activity evoked by the "Feedback," defined as the time between the onset when the result of the box-opening game was revealed, to the end of the 3-s period, in both the cooperation ($200) and the competition ($150) trials (14 in each run). B) The stimulus design matrix of a run (totally 4 runs), along with the voxel time series, was presented: each run contained 7 regressors. C) Converting a 7-regressor protocol response time into a 3-regressor version: "target_trial," "other_trials," and "others_all (the rest of the 5 regressors)." "Target_trial" and "other_trials" (from fb_200 in cooperation and fb_150 in competition) looped iteratively across all the chosen trials. For example, when the 1st trial was the target, the other trials included the 2nd trial to the last trial; when the 2nd trial was the target, the other trials were the 1st, and the 3rd to the end, and so on. D) The design matrix for a single deconvolutional GLM was created, with 8 stick-like extensions for each of the 2 regressors ("target_trial" and "other_trials"). This method allowed a least-square separation of the target trial, from which the whole-brain beta series were independently estimated subsequently for the 8 TRs following the feedback-initiated event (cooperation condition here). E) Concatenating all the 8 TRs from each trial, resulting in 448 volumes (8 TRs × 14 trials [each run] × 4 runs) for each condition, as the periodic data format ready for coherence analysis. F) The rTPJ was the seed ROI for the interpersonal seed-brain coherence analysis; thus, the regions with high coherence were mapped.

(4) con_150_2nd = "condition NT$ 150 in the competition condition, 2nd as the Receiver";

(5) fb_200 = "feedback NT$ 200 in the cooperation condition";

(6) fb_150 = "feedback NT$ 150 in the competition condition"; and

(7) others.

As the next step of the Turner method procedure, the 2 regressors (5) fb_200 and (6) fb_150, which contained 14 feedbacks in the cooperation condition (fb_200) and 14 feedbacks in the competition condition (fb_150), were kept, and the remaining 5 regressors (1, 2, 3, 4, and 7) all went into the "others_all" regressors. Therefore, the new stimulus protocol became a 3-regressor version, with "target_trial," "other_trials," and "others_all" (see Fig. 2C). In other words, both "target_trial" and "other_trials" were feedback conditions that were about to be iterated (e.g. 1 target_trial vs. the other 27 other_trials) 28 times for each run. For example, when the first trial was the target trial, the other trials included second trial to the last trial; when the second trial was the target trial, the other trials were the first, and the third to the end, and so on. Next, or as the step 4, the design matrix file (check the "SDM" folder under each pair in https://osf.io/f75cp/) for a single deconvolutional GLM (also in the "GLM" folder) with 8 stick-like finite impulse response (FIR) functions for each of the 2 regressors ("target_trial" and "other_trials") was iteratively created 28 times (Fig. 2D) (Turner et al. 2012), with the "others_all" regressor ignored. This method allows a least-square estimate of the 8 beta series (after the target trial feedback), separated from the similar estimates of the remaining 27 trials (also 8 beta series). And this process iterated 28 times for the 28 target trials in each run (Fig. 2D). As shown in Fig. 2E, the 8 first estimated beta series from each target trial (14 per condition, repeated for 4 runs) were concatenated (leaving other_trials unanalyzed), resulting in 448 whole-brain volumes per condition (8 TRs × 14 trials × 4 runs) and per subject, as the input data format for the later coherence analysis. It was worth pointing out that before the ROI–ROI or seed-to-brain coherence analysis, the volume time series were preprocessed (interpolated) with a set of Slepian tapers, resulting in multiple overlapping (75% overlap) then collapsing beta volumes. This process was as equivalent as applying a spectral smoothing of 0.005 Hz, before spectral estimation and calculation of the magnitude squared coherence.

Lastly, as shown in Fig. 2F, either rTPJ or rSTG was chosen as the seed ROIs of the current study for the interpersonal seed-brain coherence analysis. The ROI beta series were extracted from the previously concatenated beta series (448 volumes) and applied to either the ROI or whole brain of the other subject (from within-pair or the permuted pair; detailed next). In addition to the ROI–ROI coherence values, another index of Fourier decomposition, the phase-locked value, was also carried out (see Supplementary Fig. 4). These coherence-related analyses were performed in the FieldTrip toolbox (https://www.fieldtriptoolbox.org/).

Interpersonal seed-brain coherence analysis

We revised the codes from the FieldTrip website (https://www.fieldtriptoolbox.org/example/correlation_analysis_in_fmri_data/, also see CODES_and_OTHERS folder in each pair, under https://osf.io/f75cp/) as follows: First, the groupwise whole-brain mask, derived from averaging over the whole 66 participants, had 53,207 voxels and was divided into 54 segments (every 1,000 voxels for each, and the 54th with 207 voxels) because computing a seed-to-whole-brain coherence at one time will exceed the memory capacity limit of our windows PC server. Therefore, such computation was divided into 54 segmented jobs (53 * 1,000 voxels + the 54th time with 207 voxels) for each pair (check the "Coherence" folder in each pair of https://osf.io/f75cp/). Second, the rTPJ seed was downloaded from Neurosynth.org (comprising 103 published studies, with z scores 8.82, which corresponds to FDR = 0.01, under the "association test" option). The reason why only rTPJ was chosen/reported, out of many other ROIs, was primarily motivated by comparing with the only hyperscanning fMRI study with coherence analysis (i.e. Stolk et al. 2014), for the proof of concept. More importantly, the rTPJ has been heavily implicated with social cognition (Carter and Huettel 2013) and theory of mind processing (Igelström and Graziano 2017), thereby legitimizing its being chosen as the first and the most important ROI to be used here.

Third, the beta values from the seed ROI (rTPJ) were extracted and averaged (across the voxels within the ROI) for each participant. Extended analyses with rSTG as the seed ROI were also added in Supplementary Fig. 3 (for comparison and extension purposes). The coherence analysis was carried out by FieldTrip's ft_connectivity command, with the input format organized by its data structure: label, time, and trials. The outputs of coherence analysis contained 224 frequency bins (see Fig. 2F), as defined by: 0.5 (fMRI sampling frequency)/448(volumes)/2 (maximal resolution given the Nyquist equation) = 224 steps. Since each trial contained 8 beta series (TR = 2 sec), the 56th (1/16 s = 0.0625 Hz) was chosen as the designated frequency of interest. For completeness, Supplementary Video 1 contained 2 separate movies: one for the cooperation condition and the other for the competition condition. Each movie consisted of the 224-bin whole brain coherence maps (see "VMP" folder of each pair under https://osf.io/f75cp/).

For the correction over multiple comparisons over the whole brain, the coherence value was set at 0.15, and the cluster threshold 40 voxels, by the combined consideration of reasonable resulting cluster numbers and the 3dClustSim output of 36.4–40.1 voxels (either in the whole-brain mask or in the 58 × 40 × 46 voxels cases) under the $p05$ uncorrected level, NN3 definition (most lenient), and 1-sided comparison (appropriate when

coherence being always >0) under Analysis of Functional Neuroimaging (Cox 1996).

Statistical inference at the group level

Pair specificity of beta series synchronization was tested by comparing interpersonal cerebral coherence calculated on real pairs ($N = 33$ pairs) with that calculated on participants that did not share a communicative history (e.g. The Sender from the first pair with the Receiver from the second pair, and so on). For each real pair ($N = 33$), there were 32×2 random pair combinations (counting both A_{rTPJ}-$B_{brainRegion}$ and B_{rTPJ}-$A_{brainRegion}$). Therefore, the group-level *t*-tests were applied on those real versus permuted (66 vs. $33 \times 32 \times 2 = 2{,}112$) pairs. To further correct for temporal aspects of multiple comparisons, the final significance was based on "consecutive-3-significances, all at the $p01$ levels," to be counted as real $p01$ coherence at the designated frequency (see Fig. 4).

Results

Because the experiment focused on cooperation (winners divided the $200 reward) versus competition (the winner took all the $150 reward), we expected the rTPJ seed would show significant coherence with different ROIs: rSTG for the former and left precuneus (lPrecuneus) for the latter.

Behavioral results

Although the participants were never instructed on how to play, in the cooperation condition, for 99% of the time, the Receiver followed the suggestions by the Sender, who also signaled the boxes with the higher probability for 98% of the time. In contrast, the Sender in the competition condition deceived the Receiver for 45% of the trials, and the Receiver did not follow the Sender's suggestions for 43% of the time (By "deceiving," we mean that when the Sender saw the left box as with higher probability, he/she signaled the Receiver the right box as with higher probability; likewise for the "non-following" definition, when the Receiver saw the right box being highlighted, he/she picked the left box instead). These results correspond well with the predictions made by the game theory (Crawford and Sobel 1982). For other aspects of the behavioral results, please consult the relevant parts in our companion preprint (Shen et al. 2021).

Interpersonal and inter-regional coherence in the cooperation and the competition condition

Figure 3 shows the ROIs passing the corrected statistical thresholds, with mean coherence values and Talairach coordinates (see Table 1). For illustration, rSTG in the cooperation condition was chosen for its association with mutual understanding (Stolk et al. 2014), and lPrecuneus in the competition condition for its involvement during social competitions (DiMenichi and Tricomi 2017; Halko et al. 2009; Tsoi et al. 2017) as well as its specific role across distinct brain networks (Utevsky et al. 2014; Fareri et al. 2020).

Figure 4 represents the average cerebral coherence distribution between 33 pairs of the interpersonal rTPJ and rSTG (Fig. 4A, cooperation condition), and rTPJ and lPrecuneus (Fig. 4B, competition condition), based on the feedback-initiated time series (8 TR/volumes) modeled by the FIR deconvolutional analysis, or the Turner method. Especially noteworthy is the resemblance of the current Fig. 4A and Fig. 4B to the similar figure of an earlier study (cf. with Fig. 2C in Stolk et al. 2014 PNAS, pp. 18185). This coherence peak was located at the 56th frequency bin (out of $448/2 = 224$ bins), corresponding to 0.0625 Hz (1/16 s) and exactly matched the concatenated trial periodicity. These coherence peaks were identified only within the communicating (real) pairs, but not in the permuted pairs (e.g. black lines in both Fig. 4A and Fig. 4B). This is surprising given that the real and permuted pairs were identical in many aspects: the trial orders in each run, the event frequency across all 4 runs, and subjects' response time ranges, except the only difference being the shared interaction history of the real pairs, which could also be different numbers/orderings of trial outcomes. In other words, only in the simultaneously cooperating/competing pairs did the interpersonal rTPJ–rSTG/–lPrecuneus coherence emerge, but not so in randomly matched pairs where the 2 time series were drawn from different sessions. In addition, our finding also echoes the importance of STG in social interaction. Only those with shared communication history, i.e. truly interacting pairs, would more coherent activities between rTPJ and rSTG be found. This also suggests the important role of STG in social corporations, since the interpersonal rTPJ–rSTG coherence was only found in cooperation, but not in competition, conditions. Additional results are shown in the Supplementary Fig. 5, suggesting that the stronger coupling between rTPJ and rSTG in real pairs only existed during the cooperation condition, but not during the competition condition. Likewise, the stronger coupling between rTPJ and lPrecuneus in real pairs was also observed only during the competition condition, but not during the cooperation condition.

Seed-to-whole brain coherence

Figure 3 shows the seed (rTPJ) to the whole-brain interpersonal coherence maps, averaged across 66 participants, in the cooperation condition and competition condition, respectively. To be clear, these seed-to-brain coherence analyses were done prior to the seed-to-ROI coherences shown in Fig. 4A and B. As shown in Fig. 3A, medial frontal gyrus, inferior parietal lobule, postcentral gyrus, and precentral gyrus, other than rSTG, were among the brain regions that showed high interpersonal coherence with the seed rTPJ. Likewise, in Fig. 3B, middle temporal and middle frontal gyrus, other than Precuneus, were among the regions showing higher interpersonal coherence with the seed rTPJ. Table 1 provides more details of

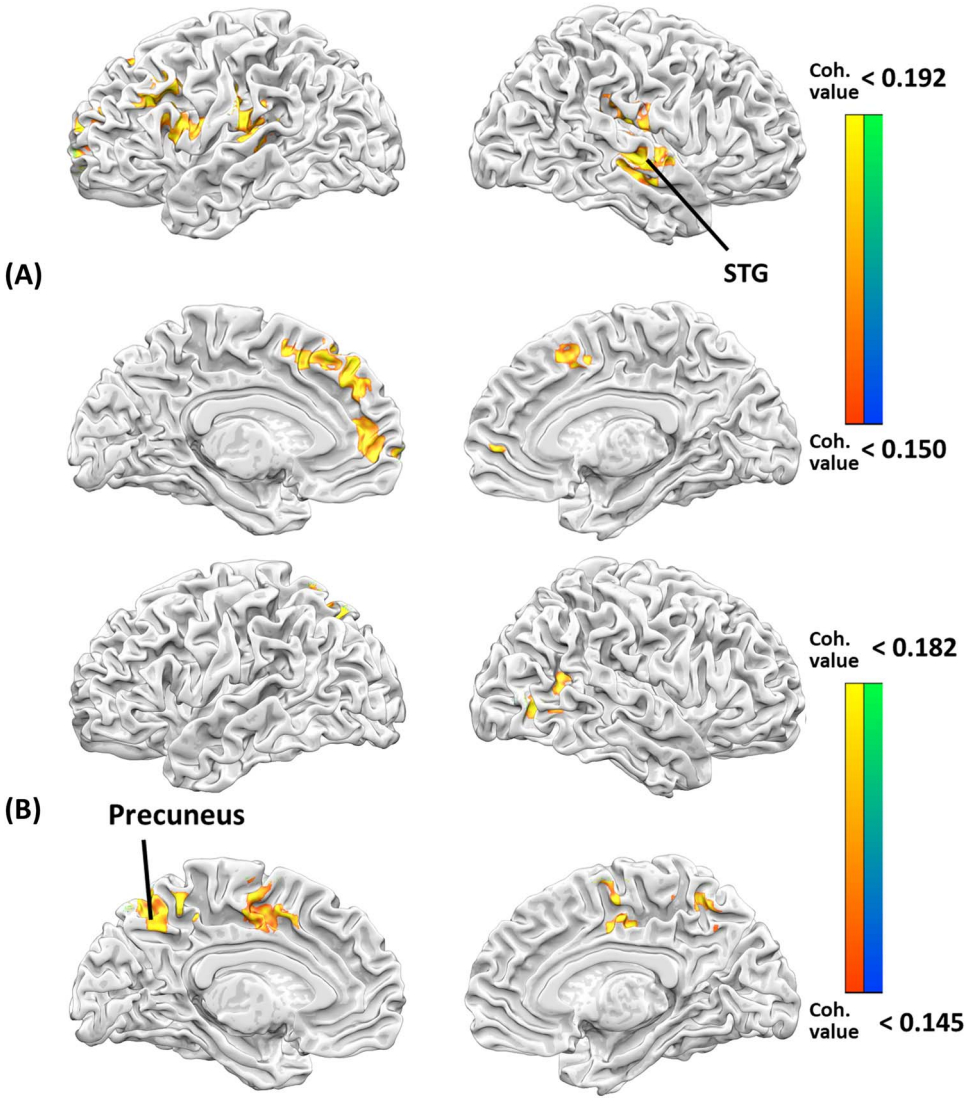

Fig. 3. The rTPJ-to-whole-brain coherence maps, both centered at the 56th frequency bin, for the cooperation (A) and the competition (B) conditions. Brain regions showed significant coherence with the rTPJ seed around the trial feedback time. A) In the cooperation condition, under the cluster *k*-threshold of 40 voxels and the applied coherence threshold of 0.15, the ROIs with significant coherence with rTPJ in the cooperation condition were postcentral gyrus, rSTG, left medial frontal gyrus, left precentral gyrus, left superior frontal gyrus, and left inferior parietal lobule. B) In the competition condition, under the cluster *k*-threshold of 40 voxels and the coherence threshold of 0.145, the coherent ROIs included left precuneus, right middle temporal gyrus, and left middle frontal gyrus.

Table 1. rTPJ-brain interpersonal coherence in cooperation and competition.

Cluster	Anatomical region	x	y	z	Coherence value
		Cooperation condition with 448 beta volumes			
Cluster 1 (voxel: 59)	R postcentral gyrus	56	−20	17	0.1885
Cluster 2 (voxel: 51)	R superior temporal gyrus	53	−24	3	0.1852
Cluster 3 (voxel: 65)	L medial frontal gyrus	−15	57	10	0.181
Cluster 4 (voxel: 85)	L precentral gyrus	−58	10	12	0.1751
Cluster 5 (voxel: 59)	L superior frontal gyrus	−8	39	42	0.1711
Cluster 6 (voxel: 58)	L inferior parietal lobule	−55	−25	27	0.1683
		Competition condition with 448 beta volumes			
Cluster 1 (voxel: 66)	L precuneus	−3	−49	49	0.1762
Cluster 2 (voxel: 46)	R middle temporal gyrus	40	−64	9	0.1684
Cluster 3 (voxel: 56)	L middle frontal gyrus	−21	−1	46	0.164

rTPJ-brain interpersonal coherence in the cooperation condition (coherence value threshold >0.15, cluster size >40 voxels threshold) and in the competition during the feedback time with 448 beta volumes (coherence value threshold >0.145, cluster size >40 voxels threshold).

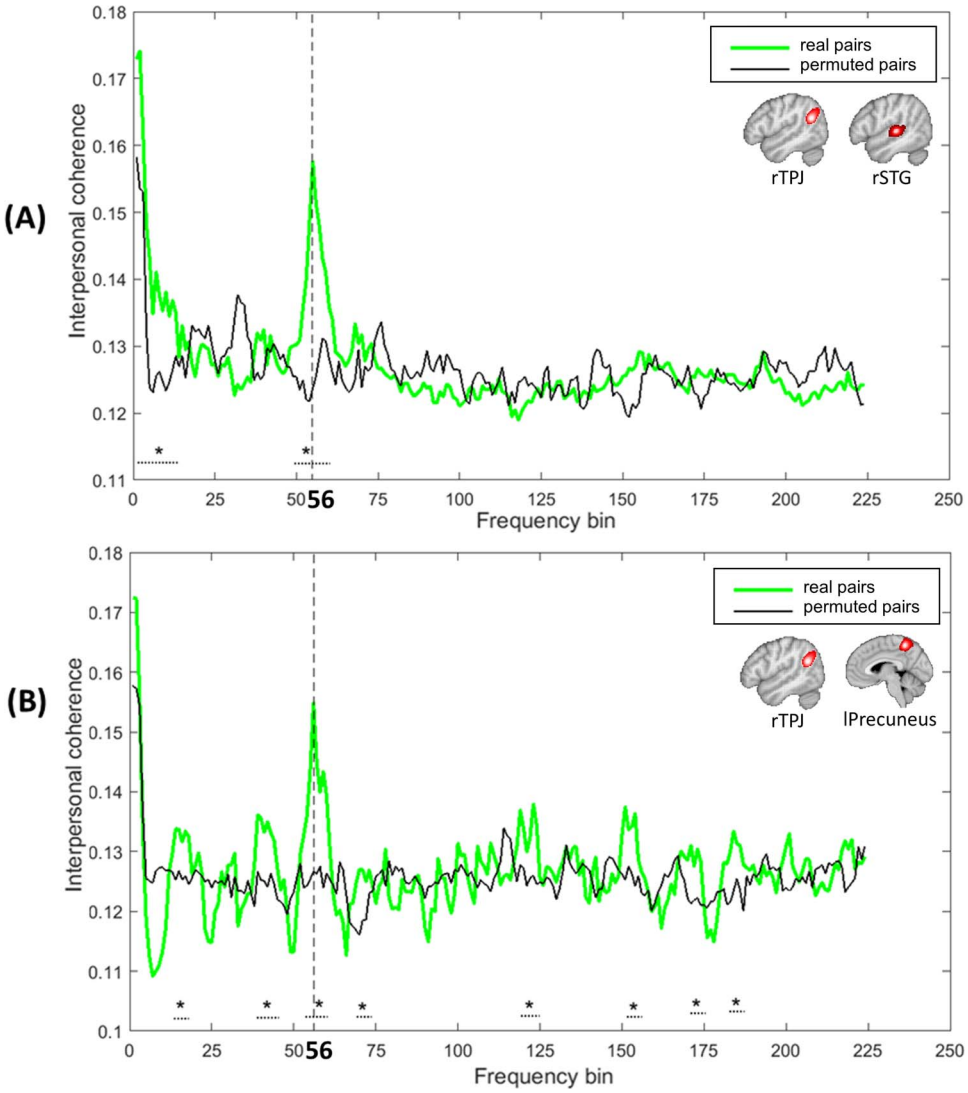

Fig. 4. Interpersonal coherence spectra. The spectra are shown between rTPJ and rSTG (A) and between rTPJ and lPrecuneus (B) of real communicative pairs (shown in green) as well as permuted pairs (shown in black) ($^{*}P > 0.01$ and 3 consecutive bins). The dominant (or peak) frequency, 0.0625 Hz (1/16 s), located at the 56th frequency bin (along the *x* axis), revealed the second highest coherence (the first bins being around time zero). This bin corresponded to the average trial frequency, as well as to the concatenated event frequency (beta series built by combining 8 betas, every 2 s/1 TR, after the trial feedback time); therefore, the heightened coherence between rTPJ–rSTG (A) and rTPJ–lPrecuneus (B) suggest that the dyads reached certain degrees of synchronization. To mitigate the false positives in many (224 frequency bins) comparisons, the group-level *t*-tests were applied on those real versus permuted (66 vs. $33 \times 32 \times 2 = 2112$) pairs, and $P = 0.01$ (a more stringent threshold) and the 3 consecutive bins (with significant differences between the real vs. permuted pairs) were both adopted as the joint significance threshold. Further evidence was provided (see Supplementary Fig. 5), to show the rTPJ–rSTG coherence "only" in the cooperation condition and the rTPJ–lPrecuneus coherence "only" in the competition condition, both in real pairs.

these clusters. These regions may be among the networks subserving the dyad interactions for both cooperation and competition.

Comparing coherences across different trial durations

To clarify whether the seed-to-ROI coherence (Fig. 4A and B) results were caused more by the 8-TR (16 s) concatenation into the event time series, or more by the close match to the average trial frequency (17 s per trial), here we created another 2 concatenated volume series with 6 and 10 TRs, or 12 and 20 s each, and repeated the coherence analyses. We reran the Turner method twice more, adapting our number of FIR sticks to 6 and 10, after the trial feedback onset. Our rationale was that if the 8-TR (16 s) coherence result was due more to the concatenated volume periodicity, then one should observe the same inter-regional coherences in the same 6-TR (or 1/12 s, 0.083 Hz) and 10-TR (1/20 s, 0.05 Hz) cases. In contrast, if the 8-TR coherence results were due more to the average trial frequency in the real fMRI data, then 6-TR or 10-TR cases should not yield the desired, or less strong, coherence, especially around the target (e.g. 56th) frequency bin. The additional rTPJ-ROI coherence analyses were carried out and plotted above/below the original 8-TR (16 s) coherence plots (Fig. 5 and Supplementary Fig. 6, respectively) for comparison purposes. The results clearly favor the contribution by the average trial frequency of the real data, rather than that by the right number of concatenated volumes, in helping shape

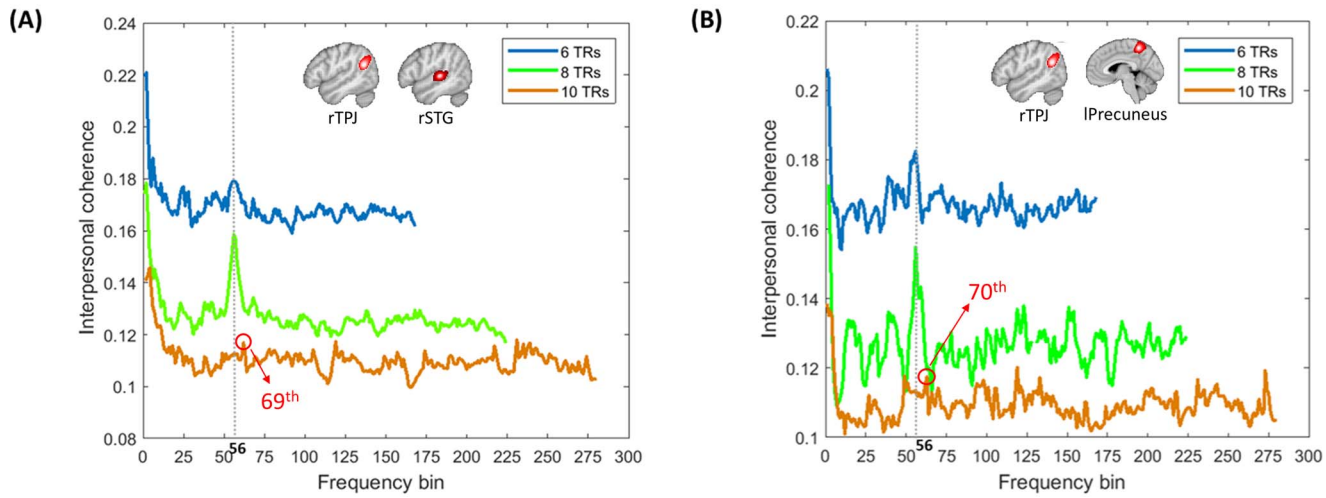

Fig. 5. Seed-to-ROI coherence mapping with the rTPJ with 6, 8, and 10 beta volumes. For both cooperation (A) and competition (B) conditions: rTPJ–rSTG or rTPJ–lPrecuneus results were presented, along with 3 kinds of TR numbers (6, 8, and 10 TRs, corresponding to 12, 16, and 20 s). The target frequency bin for 6 TR (or 1/12 s = 0.083 Hz, blue line), 8 TR (1/16 s = 0.0625 Hz, green line), and 10 TR (or 1/20 s = 0.05 Hz, brown line) were all vertically lined up at the 56th frequency bin, and the 3 frequency distributions were overlaid in a top-down manner. As can be seen in both (A) and (B), the green line showed the second highest peak at the 56th frequency bin, but less in the 6-TR (blue line) condition, much less in the 10-TR (orange line) condition. Rather, in the 10-TR condition, the real trial frequency (0.0625 Hz) was vaguely detectable at the 69th bin (or 0.0616 Hz) for the cooperation condition and the 70th bin (or 0.0625 Hz) for the competition condition, reflecting its being contaminated by other added noises (e.g. inter-trial intervals, ruminations, etc.). Both results further supported the importance of matching trial length concatenations with the average trial lengths.

the current coherence results. These analyses not only lend further support to our methodology but provide additional consideration in the coherence analysis protocol (e.g. to match the average trial frequency).

Discussion

This study aims to uncover inter-brain coherence using fMRI hyperscanning, a method that has shown a great promise in helping shape the inquiries and paradigms of social neuroscience. Despite its technical challenges, recent breakthroughs (Misaki et al. 2021) have paved ways to realize complexity underlying social dynamics, a critical component toward better understanding of human lives, as well as interactions with the earth, and the future prospect of both. As one conspicuous limitation to the application of interpersonal coherence in fMRI hyperscanning, in order to fit the periodicity requirements of frequency decompositions, the experimental design has to be adapted into regular, periodical, and full with interactions (Stolk et al. 2014; Stolk et al. 2016). Such limitations not only reduce the range of available experimental paradigms but also leave the interpretations to coherence-only dimensionality. To fill in the gap and extend the data analysts' repertoire, here we report a jittered event-related fMRI hyperscanning experiment, in where the trial-feedback responses were TR-based deconvolved into 8-volume series. With the concatenation of cooperation and competition conditions separately across runs for each participant, the final 448 (8 TRs × 14 trials × 4 runs) time series were ripe for pair-specifically or pair-randomly coherence analyses. Paralleling the past studies (Stolk et al. 2014; Stolk et al. 2016), the coherence analyses on these transformed datasets yield comparable results with Fig. 2C of Stolk et al. (2014). In a way, the realization of "having the cake and eating it too" is compellingly demonstrated, if not mentioning the additional task-based fMRI analysis, which was reported elsewhere (Shen et al. 2021).

The reported interpersonal rSTG–rSTG coherence is what Stolk et al. (2014) attributed as the source of emergent "meanings." Our findings of the rSTG-rSTG (see Supplementary Fig. 3) and the rTPJ-rSTG (see Fig. 4A) coherence in the cooperation condition, along with rTPJ-lPrecuneus (see Fig. 4B) and rSTG-other target regions in the competition conditions, all point to the general patterns of reward, execution, and theory-of-mind (ToM), -related of networks. The presence of converging rSTG–rSTG findings is encouraging, providing extra support for the notion of rSTG as the target of "conceptual alignment" (Stolk et al. 2016), but the implication behind rTPJ–rSTG is less clear. Here we propose that even though the rTPJ, the alluded target area for ToM, would be less of a degree to the level of "mutual understanding," the rTPJ–rSTG coherence still represents a second-best approximation of mutual rapport. Under the 7 computations behind social neuroscience (Molapour et al. 2021), this could be akin to the "social perception and social inference" stages that underlie social trust/rapport.

While we cannot confidently conclude what drove the rTPJ–rSTG/–lPrecuneus couplings exactly, some of the possible reasons may lie behind the couplings. Although the interacting pairs collaborated 99% of all the trials in the cooperation condition, the winning outcomes were only 75% of the time. In other words, there was only 62.5% on average that any permuted pair would receive identical reward histories. Therefore, the difference between identical feedback in the real pairs

(100%) versus the expected (62.5%) identical feedbacks in permuted pairs seem to be involved with the different coherence results. Furthermore, such feedback history differences also seem to be different in the competition condition, that is the rTPJ–lPrecuneus coherence results. It was again (100% anticorrelated, one won and the other lost) identical in real pairs versus (50%) near chance in permuted pairs. Therefore, the "different feedback" hypothesis, though currently not a viable alternative explanation, was at least partially compatible with the proposed "specific interaction histories" hypothesis. From the shared identical features between the real and permuted pairs, including the same trial orders in each run, the same trial frequency (17 s per trial) for all the 4 runs, ranges of subjects' response times (averagely, senders <1.5 s, receivers <1 s), and $^3/_4$ of the trials being "winning" in the cooperation conditions (by the game design), the only known difference was the specific interaction history in the real pairs. In other words, only in the simultaneously cooperating/competing pairs was the interpersonal rTPJ-rSTG/-lPrecuneus coherence was found. Therefore, we surmise that the answer to "what drove the coupling of the current rTPJ-rSTG/-lPrecuneus coherence results" would be: The mental processes involved during the specific interaction histories between the real interacting dyads, including (but not limited to) "implicit understandings," "mutual rapport transferring," "emotion/memory updates," or "personality attributions."

In the current study, we did not model other task events (e.g. the decision duration of senders or receivers), but only applied the FIR modeling to the feedback time because this period, upon showing the outcome of each trial, reflected the common appreciation for the reward and subsequent planning for the next trial (cooperation or competitions, etc.). In theory, the FIR-based approach could be flexibly applied to any task event including the Sender's decision versus the Receiver's decision, etc. While it may reveal certain synchronization across brain areas, certain conditional contrasts, or even multivariate analyses, these inquiries await future endeavors. Therefore, future researchers can try the coherence analysis between, such as the trial onset for the possible "joint attention" area(s), or between the Sender's and the Receiver's decisions. For the current study, our interest was more on the feedback processes where the "mutual inferred rapport" was more likely to occur.

Prior studies regarding interpersonal interactions have adopted various methods investigating the role of rTPJ and related brain areas (such as rTPJ/STG/superior temporal sulcus, or STS). For example, Abe et al. (2019) adopted multivariate autocorrelation models to assess how rTPJ's activation and its connectivity to other areas of the brain were correlated with the root mean square error between hyperscanning dyads' grip forces in collaboration. Bilek et al. (2015) used groupwise independent component analysis for identifying activities in rTPJ as sources of important components only found in interacting pairs during fMRI hyperscanning of the joint attention task, and the same fMRI data were later reanalyzed with pairwise directional coherence (Goelman et al. 2019) and confirmed rTPJ's role mainly in the receiving process during the information exchanging. Using fNIRS, Tang et al. (2016) found increased interpersonal brain coherences during face-to-face ultimatum games between pairwise rTPJs, highlighting its importance in collaborative social interactions. With EEG hyperscanning, Jahng et al. (2017) provided evidence in neural dynamics between dyads when nonverbal cues involving the rTPJ were adopted to predict opponents' intentions to cooperate or defect during the face-to-face prisoner's dilemma game. All the abovementioned studies adopted either specialized analysis methods or additional cues, such as eye contacts (Bilek et al. 2015) and facial co-analysis between patients and clinicians (Ellingsen et al. 2020) in their analyses of the information flow. The common mechanism of interpersonal rapport triggering similar brain activities should be a common theme (Cavanna and Trimble 2006; Hasson and Frith 2016; Arora et al. 2017). Together, the recent literature suggests the importance of neuron oscillations at specific frequencies (Baria et al. 2011; Benedetto et al. 2021) and decreased gamma-band in the competitive pairs (Zhou et al. 2021), both of which lend support to the "communication-through-coherence" hypothesis (Fries 2015). Therefore, coherence between two neuronal groups, brain areas, pairs, organizations, societies, or even countries or cultures could be exploited to reach effective communication, benefiting the future of human societies.

One recent comment with the title "Hyperscanning: beyond the hype" of coherence in hyperscanning fEEG/fNIRS studies listed several cautionary points that challenged the interpretations of cross-brain coherence data (Hamilton 2021). Indeed, coherence may still be epiphenomenal given that fMRI has been traditionally considered to be a correlational research tool; meanwhile, hypotheses would be best corroborated by the Multi-Brain Stimulation (or MBS) methods (Novembre and Iannetti 2020). That is, as the current study exemplifies the availability of coherence with the typical task-based fMRI, hyperscanning fMRI, with its technical advancements and methodological improvement (Misaki et al. 2021), will possibly even correlate with subject/condition-wise variables, continue to thrive for significant breakthroughs, and uncover more neural underpinnings of common or subtle within- or between-individual/group dynamics.

Acknowledgments

We thank the NCKU Mind Research and Imaging Center (MRIC) at NCKU, and the imaging center for integrated Body, Mind, and Culture research at the NTU, for the generous support and equipment availability for this collaboration. Special thanks go to Siao-Shan Shen and

HanShin Jo for comments on the analysis code, and Yi-Ching Chang, Chi-Lin Yu, Hsiang-Yun Hsiao, Tsun-Kai Chang, and all the hyperscanning team for carrying out the experiment, as well as the preprocessing of fMRI data.

Supplementary material

Supplementary material is available at *Cerebral Cortex* online.

Funding

This work was supported by funding from the Ministry of Science and Technology, Taiwan (MOST-107-2420-H-006-007-/MOST-108-2420-H-006-001-/MOST-109-2420-H-006-002- to M-HW).

Conflict of interest statement. The authors declare no competing interests.

Author contributions

C-CK, D-YC, and M-HW planned the research. D-YC, J-TC, and I-JH performed the experiments. L-SW, C-CK, D-YC, and MHW analyzed the data. L-SW, SL, C-CK, D-YC, and M-HW wrote the paper.

References

Abe MO, Koike T, Okazaki S, Sugawara SK, Takahashi K, Watanabe K, Sadato N. Neural correlates of online cooperation during joint force production. *NeuroImage*. 2019:191:150–161.

Ahn S, Cho H, Kwon M, Kim K, Kwon H, Kim BS, Chang WS, Chang JW, Jun SC. Interbrain phase synchronization during turn-taking verbal interaction—a hyperscanning study using simultaneous EEG/MEG. *Hum Brain Mapp*. 2018:39(1):171–188.

Arora A, Schurz M, Perner J. Systematic comparison of brain imaging meta-analyses of ToM with vPT. *Biomed Res Int*. 2017: 2017:6875850.

Baillet S. Magnetoencephalography for brain electrophysiology and imaging. *Nat Neurosci*. 2017:20(3):327–339.

Baria AT, Baliki MN, Parrish T, Apkarian AV. Anatomical and functional assemblies of brain BOLD oscillations. *J Neurosci*. 2011:31(21):7910–7919.

Benedetto A, Binda P, Costagli M, Tosetti M, Morrone MC. Predictive visuo-motor communication through neural oscillations. *Curr Biol*. 2021:31(15):3401–3408.e4.

Bilek E, Ruf M, Schäfer A, Akdeniz C, Calhoun VD, Schmahl C, Demanuele C, Tost H, Kirsch P, Meyer-Lindenberg A. Information flow between interacting human brains: identification, validation, and relationship to social expertise. *Proc Natl Acad Sci*. 2015:112(16):5207–5212.

Carter RM, Huettel SA. A nexus model of the temporal-parietal junction. *Trends Cogn Sci*. 2013:17(7):328–336.

Cavanna AE, Trimble MR. The precuneus: a review of its functional anatomy and behavioural correlates. *Brain*. 2006:129(3):564–583.

Chholak P, Kurkin SA, Hramov AE, Pisarchik AN. Event-related coherence in visual cortex and brain noise: an MEG study. *Appl Sci*. 2021:11(1):375.

Cox RW. AFNI: software for analysis and visualization of functional magnetic resonance neuroimages. *Comput Biomed Res*. 1996:29(3): 162–173.

Crawford VP, Sobel J. Strategic information transmission. *Econometrica*. 1982:50:1431–1451.

Czeszumski A, Eustergerling S, Lang A, Menrath D, Gerstenberger M, Schuberth S, Schreiber F, Rendon ZZ, König P. Hyperscanning: a valid method to study neural inter-brain underpinnings of social interaction. *Front Hum Neurosci*. 2020:14:39.

DiMenichi BC, Tricomi E. Increases in brain activity during social competition predict decreases in working memory performance and later recall. *Hum Brain Mapp*. 2017:38(1):457–471.

Ellingsen D-M, Isenburg K, Jung C, Lee J, Gerber J, Mawla I, Sclocco R, Jensen KB, Edwards RR, Kelley JM. Dynamic brain-to-brain concordance and behavioral mirroring as a mechanism of the patient-clinician interaction. *Sci Adv*. 2020:6(43):eabc1304.

Fareri DS, Smith DV, Delgado MR. The influence of relationship closeness on default-mode network connectivity during social interactions. *Soc Cogn Affect Neurosci*. 2020:15(3):261–271.

Fries P. Rhythms for cognition: communication through coherence. *Neuron*. 2015:88(1):220–235.

Goelman G, Dan R, Stößel G, Tost H, Meyer-Lindenberg A, Bilek E. Bidirectional signal exchanges and their mechanisms during joint attention interaction–a hyperscanning fMRI study. *NeuroImage*. 2019:198:242–254.

Halko M-L, Hlushchuk Y, Hari R, Schürmann M. Competing with peers: mentalizing-related brain activity reflects what is at stake. *NeuroImage*. 2009:46(2):542–548.

Hamilton AFC. Hyperscanning: beyond the hype. *Neuron*. 2021:109(3): 404–407.

Hasson U, Frith CD. Mirroring and beyond: coupled dynamics as a generalized framework for modelling social interactions. *Philos Trans R Soc B Biol Sci*. 2016:371(1693):20150366.

Igelström KM, Graziano MSA. The inferior parietal lobule and temporoparietal junction: a network perspective. *Neuropsychologia*. 2017:105:70–83.

Jahng J, Kralik JD, Hwang D-U, Jeong J. Neural dynamics of two players when using nonverbal cues to gauge intentions to cooperate during the Prisoner's Dilemma Game. *NeuroImage*. 2017:157: 263–274.

King-Casas B, Tomlin D, Anen C, Camerer CF, Quartz SR, Montague PR. Getting to know you: reputation and trust in a two-person economic exchange. *Science*. 2005:308(5718):78–83.

Misaki M, Kerr KL, Ratliff EL, Cosgrove KT, Simmons WK, Morris AS, Bodurka J. Beyond synchrony: the capacity of fMRI hyperscanning for the study of human social interaction. *Soc Cogn Affect Neurosci*. 2021:16(1–2):84–92.

Molapour T, Hagan CC, Silston B, Wu H, Ramstead M, Friston K, Mobbs D. Seven computations of the social brain. *Soc Cogn Affect Neurosci*. 2021:16(8):745–760.

Montague PR, Berns GS, Cohen JD, McClure SM, Pagnoni G, Dhamala M, Wiest MC, Karpov I, King RD, Apple N. Hyperscanning: simultaneous fMRI during linked social interactions. *NeuroImage*. 2002:16: 1159–1164.

Mu Y, Guo C, Han S. Oxytocin enhances inter-brain synchrony during social coordination in male adults. *Soc Cogn Affect Neurosci*. 2016:11(12):1882–1893.

Mumford JA, Turner BO, Ashby FG, Poldrack RA. Deconvolving BOLD activation in event-related designs for multivoxel pattern classification analyses. *NeuroImage*. 2012:59(3):2636–2643.

Nguyen T, Schleihauf H, Kayhan E, Matthes D, Vrtička P, Hoehl S. The effects of interaction quality on neural synchrony during mother-child problem solving. *Cortex*. 2020:124:235–249.

Novembre G, Iannetti GD. Hyperscanning alone cannot prove causality. Multibrain stimulation can. *Trends Cogn Sci*. 2020:25(2): 96–99.

Novembre G, Knoblich G, Dunne L, Keller PE. Interpersonal synchrony enhanced through 20 Hz phase-coupled dual brain stimulation. *Soc Cogn Affect Neurosci*. 2017:12(4):662–670.

Redcay E, Schilbach L. Using second-person neuroscience to elucidate the mechanisms of social interaction. *Nat Rev Neurosci*. 2019:20(8):495–505.

Shen S-S, Cheng J-T, Hsu Y-R, Chen D-Y, Weng M-H, Kung C-C. Collaborations and deceptions in strategic interactions revealed by hyperscanning fMRI. *bioRxiv*. 2021:2021.07.11.451985.

Spence M. Job market signaling the. *Q J Econ*. 1973:87(3):355–374.

Stolk A, Noordzij ML, Verhagen L, Volman I, Schoffelen J-M, Oostenveld R, Hagoort P, Toni I. Cerebral coherence between communicators marks the emergence of meaning. *Proc Natl Acad Sci*. 2014:111(51):18183–18188.

Stolk A, Verhagen L, Toni I. Conceptual alignment: how brains achieve mutual understanding. *Trends Cogn Sci*. 2016:20(3):180–191.

Tang H, Mai X, Wang S, Zhu C, Krueger F, Liu C. Interpersonal brain synchronization in the right temporo-parietal junction during face-to-face economic exchange. *Soc Cogn Affect Neurosci*. 2016:11(1):23–32.

Tsoi L, Dungan J, Waytz A, Young L. Distinct neural patterns of social cognition for cooperation versus competition. *NeuroImage*. 2017:137:86–96.

Turner BO, Mumford JA, Poldrack RA, Ashby FG. Spatiotemporal activity estimation for multivoxel pattern analysis with rapid event-related designs. *NeuroImage*. 2012:62(3):1429–1438.

Utevsky AV, Smith DV, Huettel SA. Precuneus is a functional core of the default-mode network. *J Neurosci*. 2014:34(3):932–940.

Yang J, Zhang H, Ni J, De Dreu CK, Ma Y. Within-group synchronization in the prefrontal cortex associates with intergroup conflict. *Nat Neurosci*. 2020:23(6):754–760.

Zhang D, Lin Y, Jing Y, Feng C, Gu R. The dynamics of belief updating in human cooperation: findings from inter-brain ERP hyperscanning. *NeuroImage*. 2019:198:1–12.

Zhou X, Pan Y, Zhang R, Bei L, Li X. Mortality threat mitigates interpersonal competition: an EEG-based hyperscanning study. *Soc Cogn Affect Neurosci*. 2021:16(6):621–631.